

# Med-2E3: A 2D-Enhanced 3D Medical Multimodal Large Language Model

Yiming Shi<sup>1\*</sup> Xun Zhu<sup>1\*</sup> Ying Hu<sup>1</sup> Chenyi Guo<sup>1</sup> Miao Li<sup>1†</sup> Ji Wu<sup>1,2†</sup>

<sup>1</sup> Department of Electronic Engineering, Tsinghua University

<sup>2</sup> College of AI, Tsinghua University

{sym23, zhu-x24, yinghu\_yh}@mails.tsinghua.edu.cn

{guochy, miao-li, wuji.ee}@tsinghua.edu.cn

## Abstract

The analysis of 3D medical images is crucial for modern healthcare, yet traditional task-specific models are becoming increasingly inadequate due to limited generalizability across diverse clinical scenarios. Multimodal large language models (MLLMs) offer a promising solution to these challenges. However, existing MLLMs have limitations in fully leveraging the rich, hierarchical information embedded in 3D medical images. Inspired by clinical practice, where radiologists focus on both 3D spatial structure and 2D planar content, we propose **Med-2E3**, a novel MLLM for 3D medical image analysis that integrates 3D and 2D encoders. To aggregate 2D features more effectively, we design a **Text-Guided Inter-Slice (TG-IS)** scoring module, which scores the attention of each 2D slice based on slice contents and task instructions. To the best of our knowledge, **Med-2E3** is the first MLLM to integrate both 3D and 2D features for 3D medical image analysis. Experiments on a large-scale, open-source 3D medical multimodal benchmark demonstrate that **Med-2E3** exhibits task-specific attention distribution and significantly outperforms current state-of-the-art models, with a 14% improvement in report generation and a 5% gain in medical visual question answering (VQA), highlighting the model’s potential in addressing complex multimodal clinical tasks. The code will be released upon acceptance.

## 1. Introduction

As 3D medical images become more prevalent in clinical diagnosis and treatment, the importance of 3D medical image analysis has increased, accompanied by a noticeable trend toward multimodality, diversity, and complexity. For instance, 3D medical images are now widely used in areas such as report generation, surgical planning,

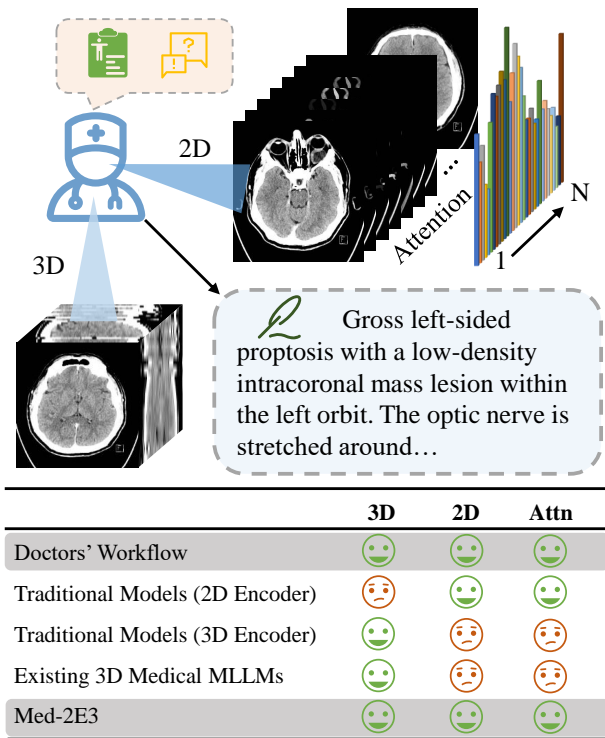


Figure 1. Radiologists typically analyze 3D medical images from both global (3D) and local (2D) perspectives, enabling them to focus on spatial structures and planar content. They allocate attention differently to slices based on their content and the specific task requirements. However, this dual-perspective feature extraction approach is often overlooked in existing models.

and beyond [7, 31, 35]. From a deep learning perspective, models for these tasks are designed to process both text and 3D medical image data, producing corresponding textual outputs. Two key tasks in this context are report generation [32, 33] and medical visual question answering (VQA) [21, 28]. For these tasks, models must have strong feature extraction and information processing capabilities to

\*Equal contribution

†Corresponding authors: Ji Wu and Miao Li

analyze complex image content and generate accurate textual information. However, traditional task-specific models [12, 36, 52] often face challenges such as limited data and small model sizes, which make it difficult to handle complex multimodal tasks.

The success of large language models (LLMs) [2, 5, 38] has greatly advanced the development of multimodal large language models (MLLMs) [3, 6, 14, 27, 30], boosting their ability to handle complex multimodal tasks. This progress has inspired researchers in the medical field to collect and build large-scale medical multimodal datasets and evaluation benchmarks, and to design, train, and evaluate medical MLLMs [26, 34, 40, 45, 46, 50]. These models have shown promising potential in addressing complex medical multimodal tasks, offering the prospect of bridging the gap between model research and clinical application.

However, existing medical MLLMs primarily focus on 2D medical images, with limited research on 3D medical MLLMs [9, 10, 13, 19]. This discrepancy may stem from the differences in data formats between 3D and 2D medical images. The data format of 2D medical images closely resembles that of natural images, enabling transfer learning using pre-trained general-purpose 2D encoders to mitigate the limited availability of medical data [16, 23, 42]. In contrast, the data format of 3D medical images differs from that of general 3D data, such as point clouds [17] and meshes [37] (although similar to video data, the time and spatial dimensions differ significantly [12]). As a result, 3D encoders must be trained from scratch on 3D medical images, which limits their representational capacity. 3D medical images typically contain rich, hierarchical information, necessitating encoders that can simultaneously model inter-slice relationships and capture intra-slice details. Existing approaches either rely on 3D encoders to directly extract whole features from 3D medical images [11, 12, 36, 44, 47, 52], or use 2D encoders to extract features slice by slice and then aggregate them [8, 20, 39, 48]. The former emphasizes modeling inter-slice relationships, thereby capturing spatial structure more effectively, while the latter focuses on intra-slice details, enabling better attention to planar content. Regardless of the approach, limitations in representation capacity persist. A critical challenge lies in building a powerful 3D medical MLLM using existing, performance-constrained encoders.

For radiologists conducting 3D medical image analysis, images are typically observed from both global and local perspectives, as shown in Fig. 1. The global perspective, akin to a 3D encoder, helps radiologists focus on the spatial structure of the image. The local perspective, similar to a 2D encoder, allows radiologists to pay attention to content within the slice plane. Given the potentially large number of slices, radiologists allocate varying levels of attention to each slice based on its content and the task requirements.

More attention is given to slices containing key organs or lesions, while irrelevant slices receive less attention. This dual perspective, combining global and local views, motivates the construction of our Med-2E3, the first MLLM to integrate both 3D and 2D encoders for 3D medical image analysis. During the aggregation of 2D features, we design a scoring module that scores the attention of each slice based on slice content and task instructions, inspired by the attention distribution mechanism used by radiologists. In summary, our contributions are as follows:

- We propose **Med-2E3**, a novel MLLM for 3D medical image analysis. To the best of our knowledge, Med-2E3 is the first 3D medical MLLM to integrate 3D and 2D encoders.
- We design a **Text-Guided Inter-Slice (TG-IS)** scoring module to mimic the attention mechanism used by radiologists in 3D medical image analysis. The module scores the attention of each slice based on slice contents and task instructions.
- Our proposed Med-2E3 achieves **state-of-the-art** performance on the largest 3D medical multimodal benchmark. It outperforms existing models in report generation, open-ended VQA, closed VQA tasks.

## 2. Related Work

### 2.1. 3D Medical Image Analysis

The development of 3D medical image analysis can be divided into two phases, marked by the emergence of LLMs [2, 5, 38]. Before the growth of LLMs, 3D medical image analysis focused primarily on relatively fixed tasks, such as classification and segmentation [12, 36, 52], which were insufficient to address the dynamic needs of clinical practice. Early multimodal tasks related to clinical applications, such as VQA, were primarily focused on 2D medical images [22, 25, 29]. The scarcity of 3D multimodal data has constrained the advancement of multimodal models for 3D medical image analysis, limiting their potential to support clinical support.

The success of LLMs has driven new advancements in the field of 3D medical image analysis [10, 15, 41]. Researchers have started collecting large-scale 3D medical multimodal datasets for model training and evaluation. Hamamci *et al.* [18] collected approximately 26K chest CT volumes along with corresponding reports, with the goal of building models specifically for chest CT data. Wu *et al.* [43] and Bai *et al.* [4] each gathered extensive 3D multimodal data from the internet, covering multiple anatomical regions and various lesions, along with associated reports and VQA data. Notably, Bai *et al.* [4] constructed M3D-Data, the largest multimodal CT dataset to date, encompassing over 100K CT volumes with corresponding reports and VQA data across various body parts, significantly advanc-

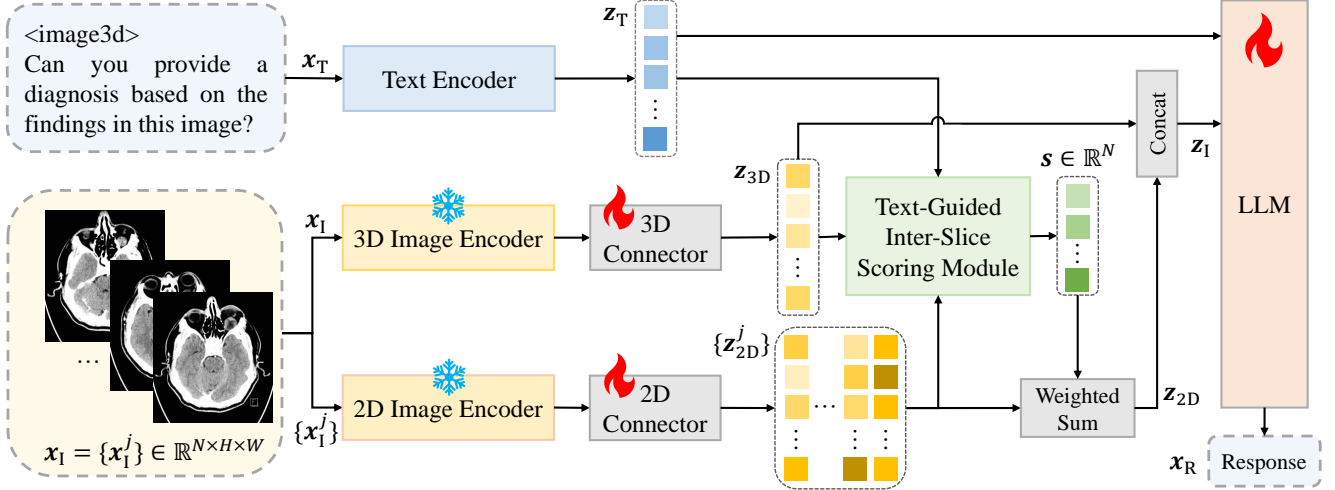


Figure 2. **Overall framework of our proposed Med-2E3.** Med-2E3 employs 3D and 2D encoders to extract complementary features ( $z_{3D}$  and  $\{z_{2D}^j\}$ ), respectively. Attention scores  $s \in \mathbb{R}^N$ , calculated by the TG-IS scoring module, are used to aggregate 2D features, which are then concatenated with 3D features. The 2D-enhanced 3D features  $z_1$  are combined with text features  $z_T$ , and the resulting input is processed by LLMs to generate the response  $x_R$ .

ing the development of 3D medical MLLMs.

Feature extraction from 3D images has long been a challenge in 3D medical image analysis. Previous research has typically followed one of two approaches. One approach involves extracting features from the entire 3D image [11, 12, 36, 44, 47, 52]. However, due to the unique modality of 3D medical images, these encoders require training from scratch on 3D data and often fail to achieve the performance levels of general-domain encoders in capturing intra-slice details. The other approach involves extracting features slice-by-slice, treating each 2D slice independently before aggregating them [8, 20, 39, 48]. While this approach allows the use of pre-trained 2D encoders fine-tuned on 3D data, it struggles to model the inter-slice relationships in 3D images.

## 2.2. Medical MLLMs

The success of MLLMs [3, 6, 14, 30] in general domains has prompted researchers to explore their medical applications. In general domains, the typical approach involves using connectors to link various modality encoders with an LLM, aligning image and text modalities during pre-training and employing instruction tuning for fine-tuning the model. The architecture and training of medical MLLMs follow a similar approach, focusing primarily on training with medical multimodal datasets. Early research on medical MLLMs has primarily focused on 2D medical images, such as Med-Flamingo [34], LLaVA-Med [26], MedVInT [50] and Uni-Med [53], which are more similar in form to natural images, with comparatively little attention given to the unique modality of 3D medical images.

As the significance of 3D medical images becomes more widely recognized, research on 3D medical MLLMs has advanced. Among existing 3D medical MLLMs, Med-BLIP [10] is designed for Alzheimer’s analysis, while 3D-CT-GPT [9], Dia-LLaMA [13], and CT-CHAT [18] specialize chest CT analysis. For broader medical applications, RadFM [43] and M3D-LaMed [4] are trained on cross-organ, multi-lesion 3D multimodal datasets. For example, M3D-LaMed first pre-trains a 3D encoder, M3D-CLIP, on a large-scale 3D medical multimodal dataset, then builds an MLLM based on the LLaVA [30] architecture, following a similar training procedure to achieve high performance. Existing 3D medical MLLMs rely primarily on 3D encoders for feature extraction. This single-encoder design does not achieve the same remarkable performance in 3D medical multimodal tasks as 2D MLLMs do in 2D multimodal tasks.

In this paper, we propose a novel MLLM, Med-2E3, which integrates both 3D and 2D encoders to address the limitations of existing 3D medical MLLMs. Specifically, we aggregate the features extracted by the 3D and 2D encoders respectively. The combination of these complementary features enables Med-2E3 to more effectively model inter-slice relationships while capturing intra-slice details.

## 3. Method

As shown in Fig. 2, this section presents the overall framework of our proposed Med-2E3. The input to Med-2E3 consists of a 3D medical image  $x_1$  and the corresponding task instructions  $x_T$ , with the output being a textual response  $x_R$ . First, as described in Sec. 3.1, Med-2E3 employs 3D, 2D, and text encoders to extract preliminary features from the

3D image and text. Next, as detailed in Sec. 3.2, a text-guided inter-slice scoring module is designed to calculate the attention scores for each slice based on these preliminary features. Finally, the 2D features are aggregated based on the attention scores and concatenated with the preliminary 3D features. These 2D-enhanced 3D features, along with the text features, are processed by the LLM to generate a response, as described in Sec. 3.3.

### 3.1. Image and Text Feature Extraction

We follow the common approach of extracting features using corresponding modality encoders for the input 3D image  $\mathbf{x}_I$  and task instructions  $\mathbf{x}_T$ . It is important to note that the features extracted at this stage are preliminary. For example, the 3D image features will undergo specially designed enhancement operations in subsequent stages.

For task instructions in textual form, a text encoder is used to extract text features  $\mathbf{z}_T$ :

$$\mathbf{z}_T = f_T(\mathbf{x}_T). \quad (1)$$

Here,  $f_T$  denotes the text encoder. In this paper, we use the LLM text embedding layer as the text encoder.

As illustrated in Fig. 2, during image feature extraction, the 3D medical image is represented in two forms: a raw form  $\mathbf{x}_I \in \mathbb{R}^{N \times H \times W}$  and a slice-based form  $\{\mathbf{x}_I^j \in \mathbb{R}^{H \times W}\}$ . The 3D and 2D feature extraction branches independently process these forms, producing complementary features  $\mathbf{z}_{3D}$  and  $\{\mathbf{z}_{2D}^j\}$ , respectively:

$$\mathbf{z}_{3D} = f_1^{(3D)}(\mathbf{x}_I), \quad (2)$$

$$\mathbf{z}_{2D}^j = f_1^{(2D)}(\mathbf{x}_I^j). \quad (3)$$

Here,  $f_1^{(3D)}$  and  $f_1^{(2D)}$  denote the 3D and 2D feature extraction branches. The 3D feature extraction branch includes a 3D image encoder and a 3D connector, while the 2D feature extraction branch consists of a 2D image encoder and a 2D connector. Superscript  $j$  represents the slice index, which ranges from 1 to  $N$ .

### 3.2. Text-Guided Inter-Slice Scoring

To mimic the attention distribution mechanism used by radiologists, we design a text-guided inter-slice (TG-IS) scoring module to score the attention of each slice based on its contents and task instructions.

First, as shown in Fig. 3, based on the position of each slice, TG-IS scoring module splits 3D features and selects relevant local features. Specifically, the serialized 1D features  $\mathbf{z}_{3D}$  are reshaped into a 3D form and the features corresponding to slice  $j$  are selected as the local features  $\mathbf{z}_{3D}^j$ . Further details are provided in the supplementary materials.

Next, the features of each slice from the 3D and 2D representations are concatenated and averaged to form slice

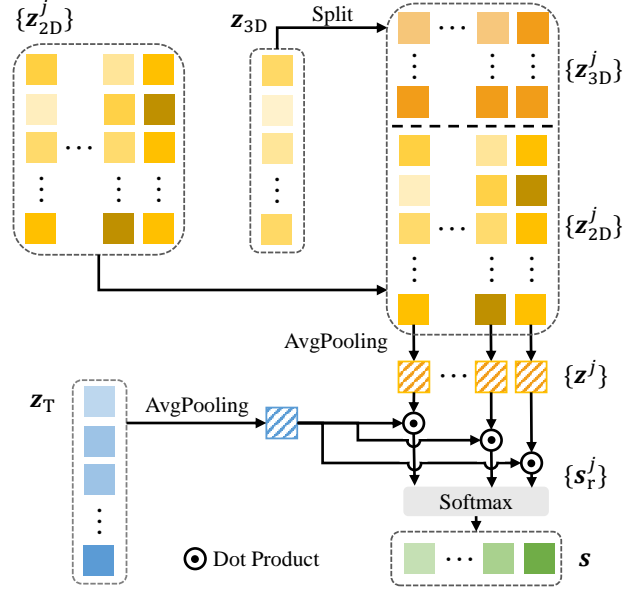


Figure 3. **Text-Guided Inter-Slice (TG-IS) Scoring Module.** The 3D features  $\mathbf{z}_{3D}$  and 2D features  $\{\mathbf{z}_{2D}^j\}$  are fused to derive the key features  $\mathbf{z}^j$  for each slice. The attention score  $\mathbf{s} \in \mathbb{R}^N$  is computed by calculating the correlation  $\{\mathbf{s}_r^j\}$  with the task instruction feature  $\mathbf{z}_T$ , followed by the softmax function for normalization.

features:

$$\mathbf{z}^j = \text{AvgPooling}([\mathbf{z}_{3D}^j; \mathbf{z}_{2D}^j]) \in \mathbb{R}^D. \quad (4)$$

Here,  $D$  denotes the feature dimension.

Since radiologists allocate varying levels of attention based on different tasks, TG-IS scoring module is designed to mimic this task-specific attention distribution. In practice, the relevance of each slice  $\mathbf{s}_r^j$  to the current task is computed by calculating the dot product between each slice’s features  $\mathbf{z}^j$  and the textual features, corresponding to the attention a radiologist would assign to each slice under the given task:

$$\mathbf{s}_r^j = \text{AvgPooling}(\mathbf{z}_T) \cdot \mathbf{z}^j. \quad (5)$$

The softmax function is then applied to normalize the relevance coefficients  $\mathbf{s}_r \in \mathbb{R}^N$ :

$$\mathbf{s} = \text{Softmax}(\mathbf{s}_r) \in \mathbb{R}^N, \quad (6)$$

to obtain the final attention score for each slice.

### 3.3. 3D Feature Enhancement

During 3D feature enhancement, to reduce computational load, the 2D features  $\{\mathbf{z}_{2D}^j\}$  extracted by the 2D branch are first aggregated based on the attention scores  $\mathbf{s} \in \mathbb{R}^N$ :

$$\mathbf{z}_{2D} = \sum_{j=1}^N \mathbf{s}^j \mathbf{z}_{2D}^j. \quad (7)$$

Next, the 3D and aggregated 2D features are concatenated to form the final features of the 3D medical image:

$$\mathbf{z}_I = [\mathbf{z}_{3D}; \mathbf{z}_{2D}]. \quad (8)$$

Finally, like most MLLMs, Med-2E3 inputs the 2D-enhanced 3D features along with the text features into the LLM, which processes them to generate the final textual response:

$$\mathbf{x}_R = f_{LLM}([\mathbf{z}_I; \mathbf{z}_T]). \quad (9)$$

## 4. Experiment

First, we describe the datasets used for training and evaluation in Sec. 4.1. Next, we provide the implementation details of Med-2E3 in Sec. 4.2. Then, we present the experimental results, comparing our proposed Med-2E3 with other MLLMs for report generation in Sec. 4.3 and medical VQA in Sec. 4.4. Finally, we conduct ablation studies in Sec. 4.5 and present case studies in Sec. 4.6.

### 4.1. Datasets

To ensure medical generalizability, we train and evaluate Med-2E3 on the large-scale 3D medical multimodal dataset, M3D-Data [4], which encompasses various organs and lesions. To ensure a fair comparison, we use only the caption and VQA data (M3D-Cap and M3D-VQA). The dataset includes over 120K CT volumes with corresponding caption and VQA annotations. M3D-VQA covers five key topics: plane, phase, organ, abnormality, and location. The multiple-choice format provides closed-ended VQA data in addition to the raw open-ended VQA data.

Following the standard training pipeline for MLLMs [4, 27, 30], we pre-train Med-2E3 to align image and text spaces, and then perform instruction tuning to fine-tune the model. We use the M3D-Cap training set, which contains 115K caption data, as the pre-training dataset. Building on this, we further incorporate the M3D-VQA training set, which consists of approximately 420K open-ended VQA and 420K closed-ended VQA data, to construct the fine-tuning dataset. For ablation studies, however, we sample the training data to balance experimental cost and efficiency. Further details are provided in Sec. 4.5.

For evaluation, we directly use the M3D-Cap and M3D-VQA test sets, which contain approximately 2K caption data, 13K open-ended VQA data and 13K closed-ended VQA data. For the caption and open-ended VQA tasks, we evaluate the similarity between generated and ground-truth text using natural language generation (NLG) metrics, including BLEU@1 (B@1), ROUGE@1 (R@1), METEOR, and BERT-Score (BERT). For the closed-opened VQA task, accuracy is calculated by comparing the predicted choices with the correct answers.

Method	B@1	R@1	M	BERT
RadFM [43]	12.23	16.49	11.57	87.93
M3D-LaMed [4]	15.15	19.55	14.38	88.46
M3D-LaMed† [4]	37.30	40.70	36.74	88.03
Med-2E3	<b>51.51</b>	<b>54.48</b>	<b>50.96</b>	<b>90.87</b>

Table 1. Evaluation results on M3D-Cap. Results with † indicate those obtained using the open-source weights. We evaluate report generation using BLEU@1 (B@1), ROUGE@1 (R@1), METEOR (M) and BERT-Score (BERT) as metrics. The best results in each column are highlighted in **bolded**.

### 4.2. Implementation Details

Our proposed Med-2E3 is built on the modular MLLMs framework TinyLLaVA [24, 51]. We use M3D-CLIP [4] as the 3D image encoder and Phi-3 [1] as the LLM, maintaining consistency with the M3D-LaMed [4] setup. For 3D feature enhancement, we incorporate a 2D image encoder, SigLIP [49], which is commonly used in recent MLLMs [24, 51].

The 3D image encoder processes inputs with a resolution of  $32 \times 256 \times 256$ , while the 2D image encoder operates at a resolution of  $256 \times 256$ . Additionally, the data pre-processing methods and training hyperparameters follow those in the M3D paper [4] to ensure fair comparisons.

All models are trained using the AdamW optimizer with bf16 mixed-precision training via DeepSpeed to enhance efficiency. The implementation is based on PyTorch and runs across two NVIDIA A800 GPUs, each with 80 GB of memory each, in parallel.

### 4.3. Evaluation on Report Generation

3D medical MLLMs evaluated on M3D-Bench (M3D-Cap and M3D-VQA) include RadFM [43] and M3D-LaMed [4]. Data and weights of M3D-LaMed are now open-sourced on HuggingFace and GitHub. Accordingly, we present both the evaluation results reported in the original paper [4], and those derived from open-source weights in Tab. 1 and Tab. 2, which are marked by †.

As shown in Tab. 1, our proposed Med-2E3 achieves state-of-the-art performance in M3D-Cap, surpassing all existing models. Specifically, Med-2E3 outperforms the best existing results by approximately 14% on BLEU@1, ROUGE@1, and METEOR metrics, and by about 2% on the BERT-Score metric.

Notably, although the training dataset of RadFM [43] is larger and covers a broader range of modalities and disease categories, its experimental results are less favorable. This may be attributed to the use of both 3D and 2D images during the training stage. Currently, there is no conclusive evidence that such a mixed data training approach positively

Method	B@1	R@1	M	BERT	Accuracy
RadFM [43]	16.39/-	26.13/-	21.33/-	88.72/-	19.79/-
M3D-LaMed [4]	49.38/-	52.39/-	33.58/-	91.53/-	75.78/-
M3D-LaMed† [4]	53.63/44.94	57.23/48.69	37.65/32.34	92.38/90.87	80.16/77.09
Med-2E3	<b>58.55/50.13</b>	<b>62.04/53.92</b>	<b>41.57/36.68</b>	<b>93.25/91.81</b>	<b>82.42/79.39</b>

Table 2. Evaluation results on M3D-VQA. We evaluate open-ended VQA using BLEU@1 (B@1), ROUGE@1 (R@1), METEOR (M) and BERT-Score (BERT) as metrics. For closed-ended VQA, we report the accuracy. Since the original M3D-VQA test set is divided into five categories based on topics, we report the averaged results. In the table, the values before and after the slash represent the macro-average and micro-average results, respectively.

Method	Report Generation				Medical VQA				
	B@1	R@1	M	BERT	B@1	R@1	M	BERT	Accuracy
3D Only	44.97	47.55	44.19	89.31	37.50	40.66	26.42	89.56	70.13
2D Only	36.96	39.63	35.78	87.65	39.22	42.48	27.83	89.84	71.71
3D + 2D	<b>49.67</b>	<b>52.12</b>	<b>48.92</b>	<b>90.25</b>	<b>39.83</b>	<b>43.13</b>	<b>28.27</b>	<b>89.95</b>	<b>72.05</b>

Table 3. Evaluation results in ablation studies of models using only 3D or 2D encoders, and the model combining 3D and 2D encoders for feature extraction. The evaluation tasks include report generation, open-ended VQA, and closed-ended VQA.

impacts the model performance in 3D medical image analysis.

#### 4.4. Evaluation on Medical VQA

In the original M3D-VQA evaluation, results for the five different VQA topics were assessed individually [4]. In our experiments, we report the overall average in Tab. 2. Due to varying sample sizes across topics, macro-average results alone would be inappropriate. Therefore, we calculated both the macro-average and micro-average results across all samples during evaluation and reported them in Tab. 2.

Our proposed Med-2E3 achieves superior performance compared to existing models in both open-ended and closed-ended VQA tasks. For the open-ended VQA task, Med-2E3 exceeds the current state-of-the-art results, improving macro-averaged and micro-averaged BLEU@1 scores by 4.92% and 5.19%, respectively; macro-averaged and micro-averaged ROUGE@1 scores by 4.81% and 5.23%; macro-averaged and micro-averaged METEOR scores by 3.92% and 4.34%; and macro-averaged and micro-averaged BERT-Score values by 0.87% and 0.94%. For the closed-ended VQA task, Med-2E3 demonstrates improvements of 2.26% and 2.3% in macro-averaged and micro-averaged accuracy, respectively, compared to the current best results. Notably, while the macro- and micro-averaged results exhibit similar overall trends, their specific values differ. In subsequent ablation studies, we report only the micro-averaged results for precision.

The exceptional performance in both report generation and medical VQA tasks underscores the effectiveness of our

proposed Med-2E3.

#### 4.5. Ablation Study

To balance training costs and efficiency, we sample the training data without altering the pre-training dataset. We retain 100K samples for the fine-tuning dataset. Given that the captioning task is relatively challenging and demands substantial data support, we select 50K caption samples, 25K open-ended VQA samples and 25K closed-ended VQA samples for instruction tuning.

In the ablation studies, we evaluate various image feature extraction methods to highlight the superiority of our proposed Med-2E3. Additionally, we examine different scoring module designs to validate the effectiveness of our current TG-IS scoring module.

##### Comparison of image feature extraction methods.

When comparing different image feature extraction methods, we focus on two main aspects: (1) the performance of models using 3D features alone, 2D features alone, or a combination of 3D and 2D features; and (2) the performance of models with different 2D feature aggregation methods in the combination of 3D and 2D features.

As shown in Tab. 3, the combination of 3D and 2D encoders outperforms models using only 3D or 2D encoders in both report generation and medical VQA tasks. The model using only the 3D encoder outperforms the one using only the 2D encoder in report generation tasks, while the model using only the 2D encoder outperforms the 3D-only model in medical VQA. The former phenomenon may be attributed to the similarity between the textual data used for pre-training the 3D encoder and the report format, which

Method	Report Generation				Medical VQA				
	B@1	R@1	M	BERT	B@1	R@1	M	BERT	Accuracy
Random Scores	47.24	49.88	46.47	89.80	39.21	42.46	27.67	89.89	71.26
MaxPooling	45.91	48.51	45.20	89.52	39.09	42.32	27.53	89.87	71.51
AvgPooling	48.50	51.10	47.83	90.04	39.26	42.51	27.76	89.90	71.47
TG-IS Scores	<b>49.67</b>	<b>52.12</b>	<b>48.92</b>	<b>90.25</b>	<b>39.83</b>	<b>43.13</b>	<b>28.27</b>	<b>89.95</b>	<b>72.05</b>

Table 4. Evaluation results in ablation studies of models using different 2D feature aggregation methods (all combining 3D and 2D encoders for complementary feature extraction). The four 2D feature aggregation methods are: AvgPooling, MaxPooling, weighted summation with random scores, and weighted summation with TG-IS scores.

Text	3D	2D	Report Generation				Medical VQA				
			B@1	R@1	M	BERT	B@1	R@1	M	BERT	Accuracy
	✓		<u>49.65</u>	<u>52.09</u>	<b>48.93</b>	89.67	39.51	42.75	27.82	89.94	<u>71.76</u>
		✓	42.81	45.43	41.85	88.86	38.83	42.16	27.39	89.82	71.34
	✓	✓	45.92	48.44	45.18	89.49	39.58	42.89	27.90	89.93	71.71
✓	✓		46.92	49.41	46.06	89.70	<b>39.83</b>	<u>43.12</u>	<u>28.19</u>	<b>90.00</b>	71.25
✓		✓	47.15	49.87	46.55	<u>89.84</u>	39.22	42.52	27.58	89.85	71.68
✓	✓	✓	<b>49.67</b>	<b>52.12</b>	<u>48.92</u>	<b>90.25</b>	<b>39.83</b>	<b>43.13</b>	<b>28.27</b>	<u>89.95</u>	<b>72.05</b>

Table 5. Evaluation results in ablation studies across tasks using different designs of the scoring module. Three key variables are considered: whether task instructions are used as guidance, and whether 3D or 2D features are used as local image features for the current slice. When task instruction guidance is absent, an additional linear layer is introduced for feature compression and scoring. The best results in each column are **bold**, and the second-best results are underlined.

naturally adapts it to the report generation task. The latter may result from the relative simplicity of the medical VQA tasks, where the feature extraction capabilities of the 2D encoder, pre-trained on natural images, are sufficiently robust to handle the task directly.

To reduce computational load, we perform 2D feature aggregation during image feature extraction. Even when using both 3D and 2D encoders to extract complementary features, different 2D feature aggregation methods lead to varying model performance across tasks. We consider four main methods for 2D feature aggregation: AvgPooling (computing the average at each position), MaxPooling (computing the maximum at each position), weighted summation with random scores, and weighted summation with TG-IS scores.

As shown in Tab. 4, the model employing our designed TG-IS-score-based aggregation achieves the best performance, followed by AvgPooling and Random Scores, while MaxPooling yields the lowest performance. This highlights the necessity of appropriate weighting for effective 2D feature aggregation, with our TG-IS score offering a compelling solution. Unlike random scores, AvgPooling and MaxPooling are fixed 2D feature aggregation methods. AvgPooling performs slightly better than Random Scores, while MaxPooling performs slightly worse, indicating that AvgPooling is a relatively good aggregation method, whereas MaxPooling is less effective. Random

scores, due to their inherent randomness, lead to generally unpredictable performance. Ablation studies above demonstrate the superiority of our proposed Med-2E3 that integrates 3D and 2D encoders.

#### Comparison of different scoring modules.

When evaluating different scoring module designs, we consider three main variables: (1) whether to use task instructions as guidance, (2) whether to use 3D features, and (3) whether to use 2D features as local image features for the current slice. When task instruction guidance is omitted, an additional linear layer is introduced into the scoring module to map image features directly to 1D vectors, enabling the softmax function to generate the inter-slice attention scores.

Results from Tab. 5 indicate that models incorporating the text-guided scoring module generally outperform those without it, especially when combining 3D and 2D features for intra-slice feature representation. However, the results do not consistently indicate whether 2D or 3D features are more effective for intra-slice representation, although 3D features appear to be slightly more significant. These ablation study results validate the effectiveness of our current TG-IS scoring module design.

#### 4.6. Case Study

Each CT volume in the dataset typically corresponds to eleven question-answer pairs, including one captioning

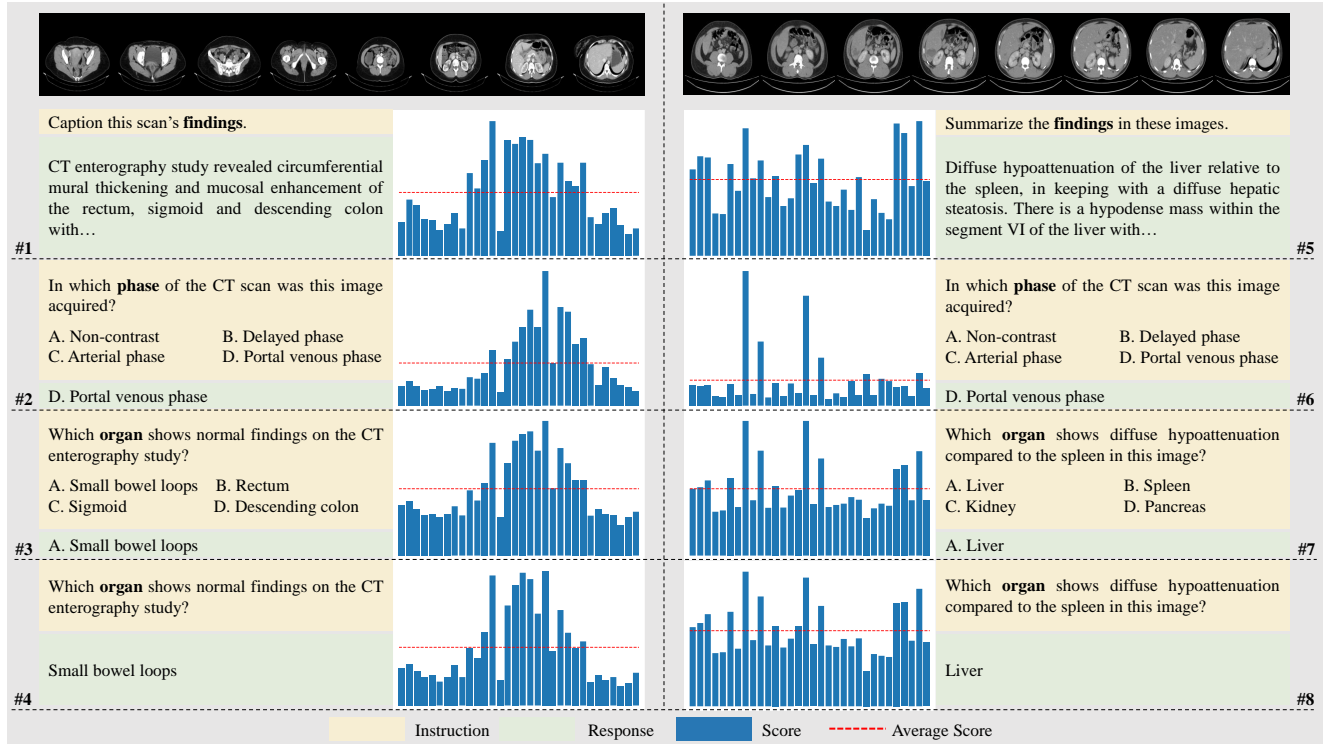


Figure 4. Visualization of two CT volumes and their corresponding question-answer pairs. To enhance clarity, we uniformly sampled 8 slices from the full CT sequence. Questions 1 and 5 correspond to report generation tasks, questions 2, 3, 6, 7 are closed-ended VQA tasks (multiple-choice questions), while questions 4 and 8 are open-ended VQA tasks (free-form questions). The keywords in each question are highlighted in **bold**. The red dashed line in the score distribution indicates the average attention score, which is 1/32.

task, five open-ended VQA tasks (free-form questions), and five closed-ended VQA tasks (multiple-choice questions), which may share the same content but differ in question formats. As shown in Fig. 4, we present two representative CT volumes and four corresponding question-answer pairs due to space constraints. Additional examples with their corresponding question-answer pairs are provided in the supplementary materials.

By comparing question pairs 1 and 5, as well as 2 and 6, we observe that although the questions are identical, the score distributions differ significantly between the two samples. This highlights the role of image feature diversity in the TG-IS scoring module. Comparing the same CT sample across different questions, we find that distinct questions yield varying score distributions, indicating that the scores are guided by task instructions, consistent with our design. Within the same sample, some slices exhibit consistent patterns or "key frames" that appear to stand out across all questions. For instance, in the right sample, certain slices consistently stand out across all questions, suggesting that these image features contribute more significantly to the scoring process.

Comparing question pairs 3 and 4, as well as 7 and 8,

we observe that although the question formats differ (one being multiple-choice and the other free-form), the content remains essentially the same, resulting in nearly identical score distributions. This demonstrates that applying AvgPooling to text feature sequences effectively produces sentence-level features. Some question score distributions are more extreme (e.g. question 6), while others are more balanced (e.g. question 8). This variance in distribution density appears to be more closely tied to the specific volume and question than to the question format. For example, although questions 2 and 6 are identical, the score distribution for question 6 is noticeably more extreme. While the score distribution for question 2 is also sparse, approximately one-third of the slices exhibit attention scores above the average.

## 5. Conclusion

In summary, we propose Med-2E3, which is the first MLLM to integrate 3D and 2D encoders for 3D medical image analysis. To aggregate 2D features effectively, we design a text-guided inter-slice (TG-IS) scoring module, computing the attention scores of different slices based on slice contents and task instructions. Med-2E3 achieves state-



of-the-art performance on the largest available multimodal benchmark for 3D medical image analysis. Med-2E3 outperforms the best existing models by 14% in report generation and by 5% in medical VQA. In addition to the excellent performance of our proposed Med-2E3, we hope that the TG-IS scoring module we designed can make the internal decision-making more transparent in the model, which could be more meaningful for clinical practice. Furthermore, we aim to provide new insights for the 3D medical image analysis research community by integrating 3D and 2D encoders to leverage complementary features.

## References

- [1] Marah Abdin, Sam Ade Jacobs, Ammar Ahmad Awan, Jyoti Aneja, Ahmed Awadallah, Hany Awadalla, Nguyen Bach, Amit Bahree, Arash Bakhtiari, Harkirat Behl, et al. Phi-3 technical report: A highly capable language model locally on your phone. *arXiv preprint arXiv:2404.14219*, 2024. 5
- [2] Josh Achiam, Steven Adler, Sandhini Agarwal, Lama Ahmad, Ilge Akkaya, Florencia Leoni Aleman, Diogo Almeida, Janko Altmenschmidt, Sam Altman, Shyamal Anadkat, et al. Gpt-4 technical report. *arXiv preprint arXiv:2303.08774*, 2023. 2
- [3] Jean-Baptiste Alayrac, Jeff Donahue, Pauline Luc, Antoine Miech, Iain Barr, Yana Hasson, Karel Lenc, Arthur Mensch, Katherine Millican, Malcolm Reynolds, et al. Flamingo: a visual language model for few-shot learning. *Advances in neural information processing systems*, 35:23716–23736, 2022. 2, 3
- [4] Fan Bai, Yuxin Du, Tiejun Huang, Max Q-H Meng, and Bo Zhao. M3d: Advancing 3d medical image analysis with multi-modal large language models. *arXiv preprint arXiv:2404.00578*, 2024. 2, 3, 5, 6
- [5] Jinze Bai, Shuai Bai, Yunfei Chu, Zeyu Cui, Kai Dang, Xiaodong Deng, Yang Fan, Wenbin Ge, Yu Han, Fei Huang, et al. Qwen technical report. *arXiv preprint arXiv:2309.16609*, 2023. 2
- [6] Jinze Bai, Shuai Bai, Shusheng Yang, Shijie Wang, Sinan Tan, Peng Wang, Junyang Lin, Chang Zhou, and Jingren Zhou. Qwen-vl: A versatile vision-language model for understanding, localization, text reading, and beyond. *arXiv preprint arXiv:2308.12966*, 1(2):3, 2023. 2, 3
- [7] Junaid Bajwa, Usman Munir, Aditya Nori, and Bryan Williams. Artificial intelligence in healthcare: transforming the practice of medicine. *Future healthcare journal*, 8(2):e188–e194, 2021. 1
- [8] Niamh Belton, Ivan Welaratne, Adil Dahlan, Ronan T Hearne, Misgina Tsighe Hagos, Aonghus Lawlor, and Kathleen M Curran. Optimising knee injury detection with spatial attention and validating localisation ability. In *Annual conference on medical image understanding and analysis*, pages 71–86. Springer, 2021. 2, 3
- [9] Hao Chen, Wei Zhao, Yingli Li, Tianyang Zhong, Yisong Wang, Youlan Shang, Lei Guo, Junwei Han, Tianming Liu, Jun Liu, et al. 3d-ct-gpt: Generating 3d radiology reports through integration of large vision-language models. *arXiv preprint arXiv:2409.19330*, 2024. 2, 3
- [10] Qiuhui Chen, Xinyue Hu, Zirui Wang, and Yi Hong. Medblip: Bootstrapping language-image pre-training from 3d medical images and texts. *arXiv preprint arXiv:2305.10799*, 2023. 2, 3
- [11] Qiuhui Chen, Huping Ye, and Yi Hong. Med3dinsight: Enhancing 3d medical image understanding with 2d multi-modal large language models. *arXiv preprint arXiv:2403.05141*, 2024. 2, 3
- [12] Sihong Chen, Kai Ma, and Yefeng Zheng. Med3d: Transfer learning for 3d medical image analysis. *arXiv preprint arXiv:1904.00625*, 2019. 2, 3
- [13] Zhixuan Chen, Luyang Luo, Yequan Bie, and Hao Chen. Dia-llama: Towards large language model-driven ct report generation. *arXiv preprint arXiv:2403.16386*, 2024. 2, 3
- [14] Zhe Chen, Jiannan Wu, Wenhai Wang, Weijie Su, Guo Chen, Sen Xing, Muyan Zhong, Qinglong Zhang, Xizhou Zhu, Lewei Lu, et al. Internvl: Scaling up vision foundation models and aligning for generic visual-linguistic tasks. In *Proceedings of the IEEE/CVF Conference on Computer Vision and Pattern Recognition*, pages 24185–24198, 2024. 2, 3
- [15] Yuxin Du, Fan Bai, Tiejun Huang, and Bo Zhao. Segvol: Universal and interactive volumetric medical image segmentation. *arXiv preprint arXiv:2311.13385*, 2023. 2
- [16] Sedigheh Eslami, Christoph Meinel, and Gerard De Melo. Pubmedclip: How much does clip benefit visual question answering in the medical domain? In *Findings of the Association for Computational Linguistics: EACL 2023*, pages 1181–1193, 2023. 2
- [17] Yulan Guo, Hanyun Wang, Qingyong Hu, Hao Liu, Li Liu, and Mohammed Bennamoun. Deep learning for 3d point clouds: A survey. *IEEE transactions on pattern analysis and machine intelligence*, 43(12):4338–4364, 2020. 2
- [18] Ibrahim Ethem Hamamci, Sezgin Er, Furkan Almas, Ayse Gulnihan Simsek, Seval Nil Esirgun, Irem Dogan, Muhammed Furkan Dasdelen, Omer Faruk Durugol, Bastian Wittmann, Tamaz Amiranashvili, Enis Simsar, Mehmet Simsar, Emine Bensus Erdemir, Abdullah Alanbay, Anjany Sekuboyina, Berkan Lafci, Christian Bluethgen, Mehmet Kemal Ozdemir, and Bjoern Menze. Developing generalist foundation models from a multimodal dataset for 3d computed tomography, 2024. 2, 3
- [19] Ibrahim Ethem Hamamci, Sezgin Er, and Bjoern Menze. Ct2rep: Automated radiology report generation for 3d medical imaging. In *International Conference on Medical Image Computing and Computer-Assisted Intervention*, pages 476–486. Springer, 2024. 2
- [20] Xiao Han. Automatic liver lesion segmentation using a deep convolutional neural network method. *arXiv preprint arXiv:1704.07239*, 2017. 2, 3
- [21] Iryna Hartsock and Ghulam Rasool. Vision-language models for medical report generation and visual question answering: A review. *arXiv preprint arXiv:2403.02469*, 2024. 1
- [22] Xuehai He, Yichen Zhang, Luntian Mou, Eric Xing, and Pengtao Xie. Pathvqa: 30000+ questions for medical visual question answering. *arXiv preprint arXiv:2003.10286*, 2020. 2

- [23] Shih-Cheng Huang, Liyue Shen, Matthew P Lungren, and Serena Yeung. Gloria: A multimodal global-local representation learning framework for label-efficient medical image recognition. In *Proceedings of the IEEE/CVF International Conference on Computer Vision*, pages 3942–3951, 2021. 2
- [24] Junlong Jia, Ying Hu, Xi Weng, Yiming Shi, Miao Li, Xingjian Zhang, Baichuan Zhou, Ziyu Liu, Jie Luo, Lei Huang, et al. Tinyllava factory: A modularized codebase for small-scale large multimodal models. *arXiv preprint arXiv:2405.11788*, 2024. 5
- [25] Jason J Lau, Soumya Gayen, Asma Ben Abacha, and Dina Demner-Fushman. A dataset of clinically generated visual questions and answers about radiology images. *Scientific data*, 5(1):1–10, 2018. 2
- [26] Chunyuan Li, Cliff Wong, Sheng Zhang, Naoto Usuyama, Haotian Liu, Jianwei Yang, Tristan Naumann, Hoifung Poon, and Jianfeng Gao. Llava-med: Training a large language-and-vision assistant for biomedicine in one day. *Advances in Neural Information Processing Systems*, 36, 2024. 2, 3
- [27] Junnan Li, Dongxu Li, Silvio Savarese, and Steven Hoi. Blip-2: Bootstrapping language-image pre-training with frozen image encoders and large language models. In *International conference on machine learning*, pages 19730–19742. PMLR, 2023. 2, 5
- [28] Zhihong Lin, Donghao Zhang, Qingyi Tao, Danli Shi, Gholamreza Haffari, Qi Wu, Mingguang He, and Zongyuan Ge. Medical visual question answering: A survey. *Artificial Intelligence in Medicine*, 143:102611, 2023. 1
- [29] Bo Liu, Li-Ming Zhan, Li Xu, Lin Ma, Yan Yang, and Xiao-Ming Wu. Slake: A semantically-labeled knowledge-enhanced dataset for medical visual question answering. In *2021 IEEE 18th International Symposium on Biomedical Imaging (ISBI)*, pages 1650–1654. IEEE, 2021. 2
- [30] Haotian Liu, Chunyuan Li, Qingyang Wu, and Yong Jae Lee. Visual instruction tuning. *Advances in neural information processing systems*, 36, 2024. 2, 3, 5
- [31] Lena Maier-Hein, Swaroop S Vedula, Stefanie Speidel, Nasir Navab, Ron Kikinis, Adrian Park, Matthias Eisenmann, Hubertus Feussner, Germain Forestier, Stamatia Giannarou, et al. Surgical data science for next-generation interventions. *Nature Biomedical Engineering*, 1(9):691–696, 2017. 1
- [32] Pablo Messina, Pablo Pino, Denis Parra, Alvaro Soto, Cecilia Besa, Sergio Uribe, Marcelo Andía, Cristian Tejos, Claudia Prieto, and Daniel Capurro. A survey on deep learning and explainability for automatic report generation from medical images. *ACM Computing Surveys (CSUR)*, 54(10s):1–40, 2022. 1
- [33] Maram Mahmoud A Monshi, Josiah Poon, and Vera Chung. Deep learning in generating radiology reports: A survey. *Artificial Intelligence in Medicine*, 106:101878, 2020. 1
- [34] Michael Moor, Qian Huang, Shirley Wu, Michihiro Yasunaga, Yash Dalmia, Jure Leskovec, Cyril Zakka, Eduardo Pontes Reis, and Pranav Rajpurkar. Med-flamingo: a multimodal medical few-shot learner. In *Machine Learning for Health (ML4H)*, pages 353–367. PMLR, 2023. 2, 3
- [35] Xiangdong Pei, Ke Zuo, Yuan Li, and Zhengbin Pang. A review of the application of multi-modal deep learning in medicine: bibliometrics and future directions. *International Journal of Computational Intelligence Systems*, 16(1):44, 2023. 1
- [36] Yucheng Tang, Dong Yang, Wenqi Li, Holger R Roth, Bennett Landman, Daguang Xu, Vishwesh Nath, and Ali Hatamizadeh. Self-supervised pre-training of swin transformers for 3d medical image analysis. In *Proceedings of the IEEE/CVF conference on computer vision and pattern recognition*, pages 20730–20740, 2022. 2, 3
- [37] Yating Tian, Hongwen Zhang, Yebin Liu, and Limin Wang. Recovering 3d human mesh from monocular images: A survey. *IEEE transactions on pattern analysis and machine intelligence*, 2023. 2
- [38] Hugo Touvron, Thibaut Lavril, Gautier Izacard, Xavier Martinet, Marie-Anne Lachaux, Timothée Lacroix, Baptiste Rozière, Naman Goyal, Eric Hambro, Faisal Azhar, et al. Llama: Open and efficient foundation language models. *arXiv preprint arXiv:2302.13971*, 2023. 2
- [39] Chen-Han Tsai, Nahum Kiryati, Eli Konen, Iris Eshed, and Arnaldo Mayer. Knee injury detection using mri with efficiently-layered network (elnet). In *Medical Imaging with Deep Learning*, pages 784–794. PMLR, 2020. 2, 3
- [40] Tao Tu, Shekoofeh Azizi, Danny Driess, Mike Schaeckermann, Mohamed Amin, Pi-Chuan Chang, Andrew Carroll, Charles Lau, Ryutarō Tanno, Ira Ktena, et al. Towards generalist biomedical ai. *NEJM AI*, 1(3):A10a2300138, 2024. 2
- [41] Haoyu Wang, Sizheng Guo, Jin Ye, Zhongying Deng, Junlong Cheng, Tianbin Li, Jianpin Chen, Yanzhou Su, Ziyang Huang, Yiqing Shen, Bin Fu, Shaoting Zhang, Junjun He, and Yu Qiao. Sam-med3d. *arXiv preprint arXiv:2310.15161*, 2023. 2
- [42] Zifeng Wang, Zhenbang Wu, Dinesh Agarwal, and Jimeng Sun. Medclip: Contrastive learning from unpaired medical images and text. *arXiv preprint arXiv:2210.10163*, 2022. 2
- [43] Chaoyi Wu, Xiaoman Zhang, Ya Zhang, Yanfeng Wang, and Weidi Xie. Towards generalist foundation model for radiology. *arXiv preprint arXiv:2308.02463*, 2023. 2, 3, 5, 6
- [44] Linshan Wu, Jiaxin Zhuang, and Hao Chen. Vococ: A simple-yet-effective volume contrastive learning framework for 3d medical image analysis. In *Proceedings of the IEEE/CVF Conference on Computer Vision and Pattern Recognition*, pages 22873–22882, 2024. 2, 3
- [45] Yunfei Xie, Ce Zhou, Lang Gao, Juncheng Wu, Xianhang Li, Hong-Yu Zhou, Sheng Liu, Lei Xing, James Zou, Cihang Xie, et al. Medtrinity-25m: A large-scale multimodal dataset with multigranular annotations for medicine. *arXiv preprint arXiv:2408.02900*, 2024. 2
- [46] Lin Yang, Shawn Xu, Andrew Sellergren, Timo Kohlberger, Yuchen Zhou, Ira Ktena, Atilla Kiraly, Faruk Ahmed, Farhad Hormozdiari, Tiam Jaroensri, et al. Advancing multimodal medical capabilities of gemini. *arXiv preprint arXiv:2405.03162*, 2024. 2
- [47] Yiwen Ye, Yutong Xie, Jianpeng Zhang, Ziyang Chen, Qi Wu, and Yong Xia. Continual self-supervised learning: Towards universal multi-modal medical data representation learning. In *Proceedings of the IEEE/CVF Conference on*

- Computer Vision and Pattern Recognition*, pages 11114–11124, 2024. [2](#), [3](#)
- [48] Qihang Yu, Lingxi Xie, Yan Wang, Yuyin Zhou, Elliot K Fishman, and Alan L Yuille. Recurrent saliency transformation network: Incorporating multi-stage visual cues for small organ segmentation. In *Proceedings of the IEEE conference on computer vision and pattern recognition*, pages 8280–8289, 2018. [2](#), [3](#)
- [49] Xiaohua Zhai, Basil Mustafa, Alexander Kolesnikov, and Lucas Beyer. Sigmoid loss for language image pre-training. In *Proceedings of the IEEE/CVF International Conference on Computer Vision*, pages 11975–11986, 2023. [5](#)
- [50] Xiaoman Zhang, Chaoyi Wu, Ziheng Zhao, Weixiong Lin, Ya Zhang, Yanfeng Wang, and Weidi Xie. Pmc-vqa: Visual instruction tuning for medical visual question answering. *arXiv preprint arXiv:2305.10415*, 2023. [2](#), [3](#)
- [51] Baichuan Zhou, Ying Hu, Xi Weng, Junlong Jia, Jie Luo, Xien Liu, Ji Wu, and Lei Huang. Tynllava: A framework of small-scale large multimodal models. *arXiv preprint arXiv:2402.14289*, 2024. [5](#)
- [52] Zongwei Zhou, Vatsal Sodha, Md Mahfuzur Rahman Siddiquee, Ruibin Feng, Nima Tajbakhsh, Michael B Gotway, and Jianming Liang. Models genesis: Generic autodidactic models for 3d medical image analysis. In *Medical Image Computing and Computer Assisted Intervention–MICCAI 2019: 22nd International Conference, Shenzhen, China, October 13–17, 2019, Proceedings, Part IV 22*, pages 384–393. Springer, 2019. [2](#), [3](#)
- [53] Xun Zhu, Ying Hu, Fanbin Mo, Miao Li, and Ji Wu. Uni-med: A unified medical generalist foundation model for multi-task learning via connector-moe. *arXiv preprint arXiv:2409.17508*, 2024. [3](#)

# Med-2E3: A 2D-Enhanced 3D Medical Multimodal Large Language Model

## Supplementary Material

### A. 3D Feature Transformation

In the TG-IS scoring module, complete slice features  $\{z^j\}$  are formed by dividing and reorganizing the 3D features  $z_{3D}$  into a multi-slice format  $\{z_{3D}^j \in \mathbb{R}^{L \times D}\}$ , which are then concatenated with their corresponding 2D features  $\{z_{2D}^j\}$ .

Assuming the original image size is  $N \times H \times W$ , the features extracted by the 3D encoder with a patch size of  $N_1 \times H_1 \times W_1$ , are reshaped into a 1D vector of length  $L_1$ :

$$L_1 = \frac{N}{N_1} \cdot \frac{H}{H_1} \cdot \frac{W}{W_1}. \quad (10)$$

Subsequently, the features are processed through a 3D connector with a pooling layer. Assuming the pooling operation downsamples by a factor of  $P$ , the resulting 3D features are further reduced to a 1D vector of length  $L_2$ :

$$L_2 = \frac{L_1}{P^3} = \frac{N}{N_1 \cdot P} \cdot \frac{H}{H_1 \cdot P} \cdot \frac{W}{W_1 \cdot P}. \quad (11)$$

Consequently, the final 3D features  $z_{3D}$  have a shape of  $L_2 \times D$ .

As shown in Algorithm 1, the one-dimension 3D features  $z_{3D}$  are initially reshaped into a 3D format, resulting in the following feature shape:

$$\frac{N}{N_1 \cdot P} \times \frac{H}{H_1 \cdot P} \times \frac{W}{W_1 \cdot P} \times D. \quad (12)$$

To align the first dimension with the number of 2D features  $\{z_{2D}^j\}$ , each layer of the 3D features is replicated  $N_1 \cdot P$  times. Rather than directly concatenating the replicated layers, an **interleaved concatenation** strategy is applied, resulting in the following feature shape:

$$N \times \frac{H}{H_1 \cdot P} \times \frac{W}{W_1 \cdot P} \times D. \quad (13)$$

Finally, the features are reshaped into  $N$  instances of  $z_{3D}^j$ , each with a shape of  $L \times D$ , where  $L$  is defined as:

$$L = \frac{H}{H_1 \cdot P} \times \frac{W}{W_1 \cdot P}. \quad (14)$$

### B. Case Study

As illustrated in Figs. 5 to 7, we provide three additional CT volumes together with their corresponding 11 question-answer pairs, comprising one captioning task, five open-ended VQA tasks, and five closed-ended VQA tasks. Significant variance in score is observed across different CT samples. Within the same CT sample, the score distribution

---

**Algorithm 1:** Transformation of 3D features for alignment with 2D features in the first dimension.

---

**Input:** 3D features  $z_{3D}$  of shape  $(L_2, D)$ , where

$$L_2 = \frac{N}{N_1 \cdot P} \cdot \frac{H}{H_1 \cdot P} \cdot \frac{W}{W_1 \cdot P}$$

**Output:** Transformed 3D features  $\{z_{3D}^j\}$  of shape  $(N, L, D)$ , where

$$L = \frac{H}{H_1 \cdot P} \cdot \frac{W}{W_1 \cdot P}$$

**Step 1: Reshape** the input  $z_{3D}$  into a 3D format:

$$\text{New shape} \leftarrow \left( \frac{N}{N_1 \cdot P}, \frac{H}{H_1 \cdot P}, \frac{W}{W_1 \cdot P}, D \right)$$

**Step 2: Replicate** the first dimension  $N_1 \cdot P$  times and **interleave** 3D features to match 2D features:

$$\text{Replicated shape} \leftarrow \left( N, \frac{H}{H_1 \cdot P}, \frac{W}{W_1 \cdot P}, D \right)$$

**Step 3: Reshape** interleaved features into  $N$  slices:

$$\{z_{3D}^j\} \leftarrow \text{Reshape to } (N, L, D),$$

$$\text{where } L = \frac{H}{H_1 \cdot P} \cdot \frac{W}{W_1 \cdot P}$$

**return**  $\{z_{3D}^j\}$

---

also varies across questions, highlighting the influence of the type of question on the scoring mechanism.

From a macro-perspective, each CT sample exhibits certain underlying patterns, indicating that the image features are critical in shaping the scoring process.

From a micro-perspective, while 3D features are replicated across multiple layers to align the number of 3D and 2D feature layers during the transformation process, no consistent pattern is observed in the scores of adjacent slices. This underscores the importance of 2D features in shaping the scoring process.

Questions with similar content, but presented in different formats, tend to produce comparable scores. In general, scores associated with phase-specific topics are relatively sparse, whereas scores for other questions, particularly those related to captions, are more densely distributed. This observation aligns with typical radiological practices when analyzing 3D medical images.

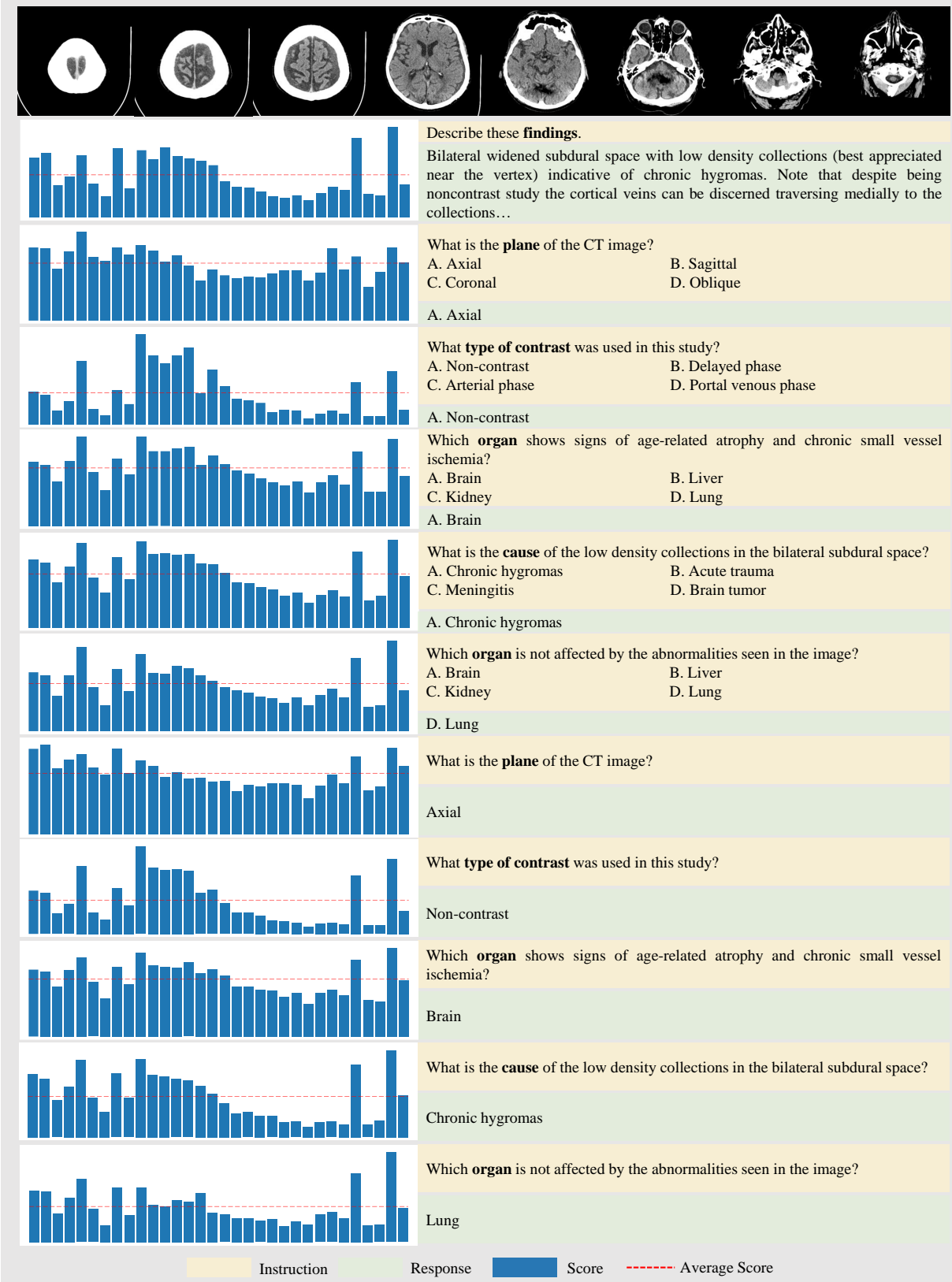


Figure 5. Visualization of a CT volume alongside its corresponding question-answer pairs.

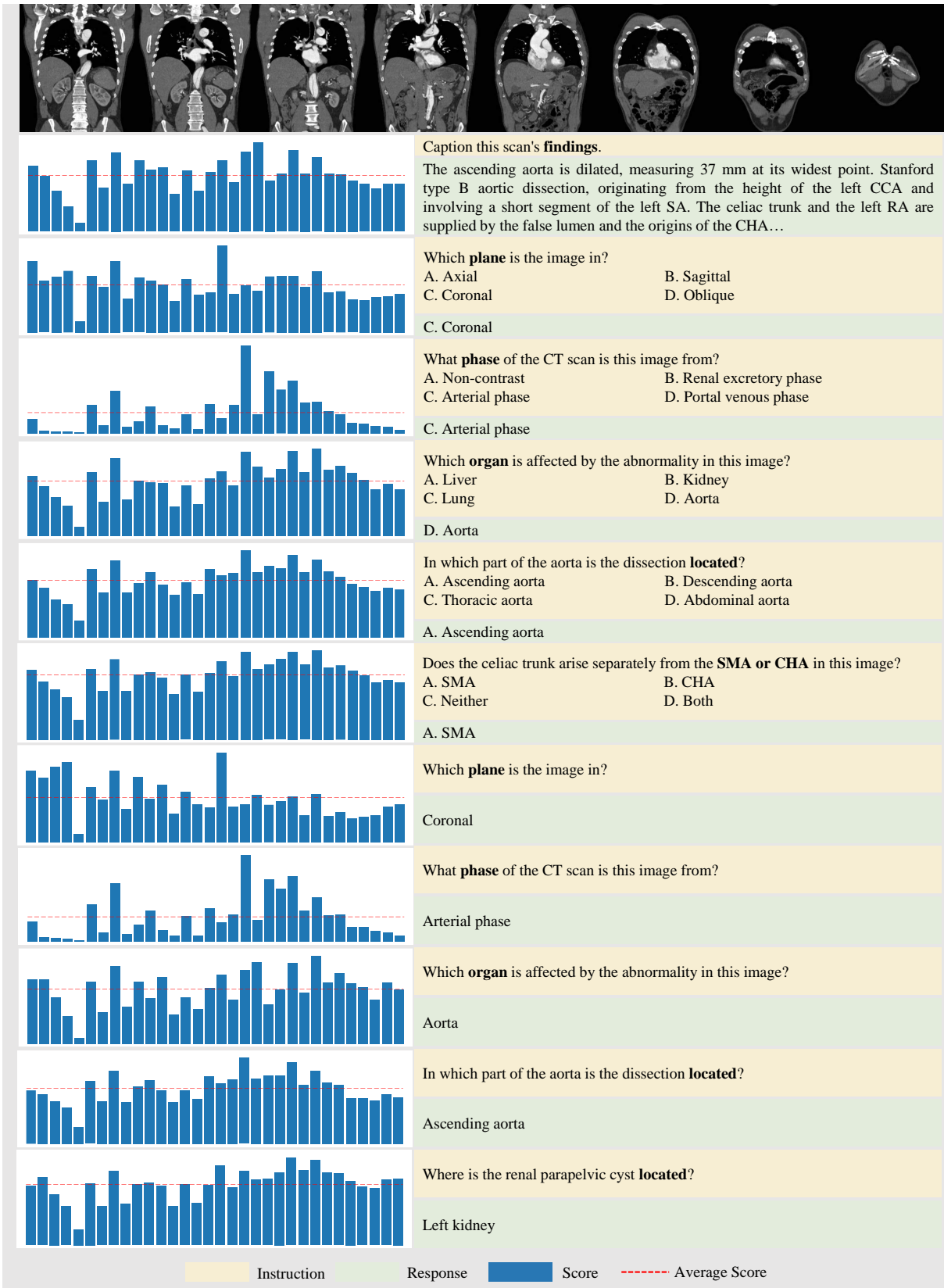


Figure 6. Visualization of a CT volume alongside its corresponding question-answer pairs.

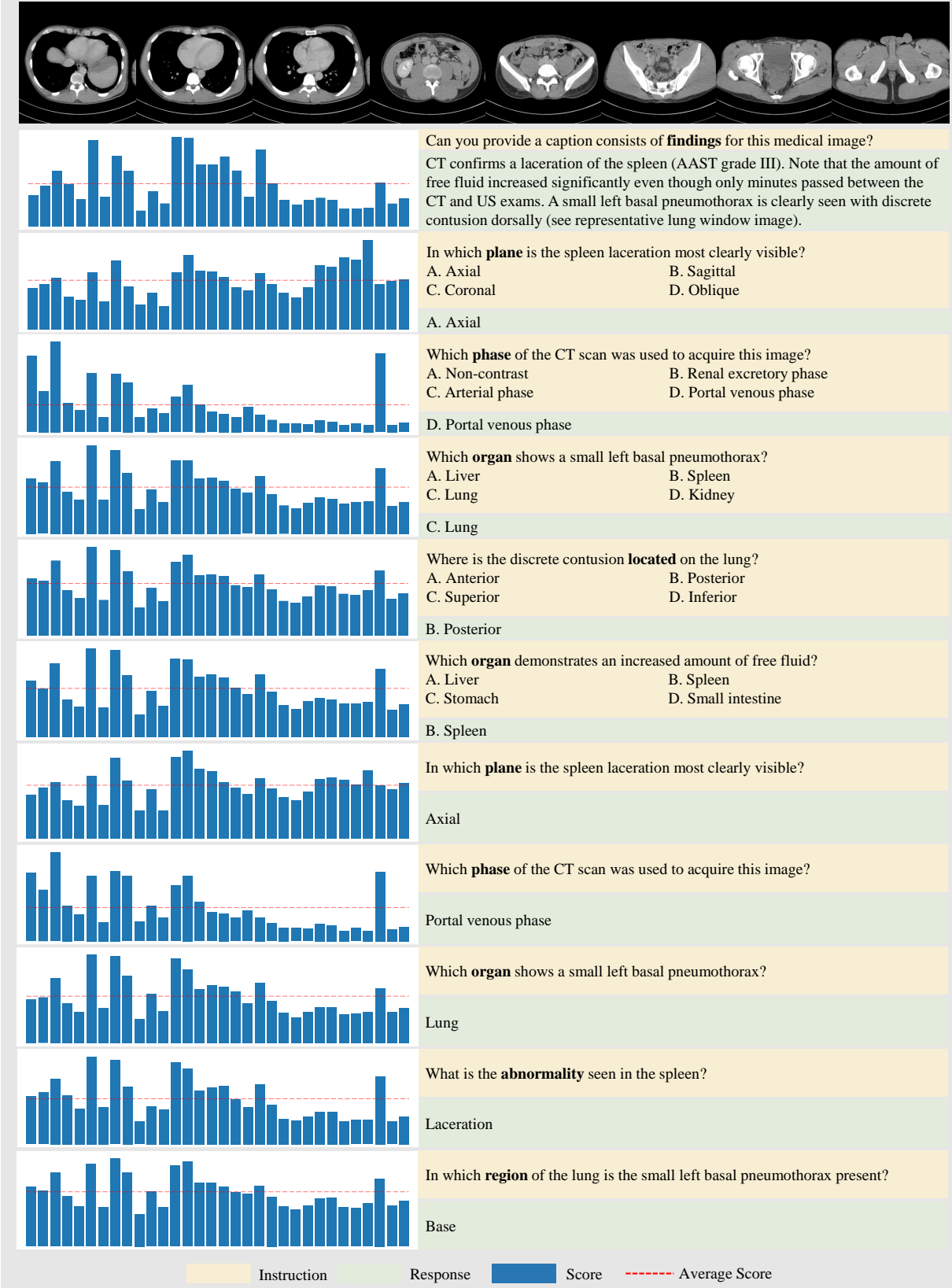


Figure 7. Visualization of a CT volume alongside its corresponding question-answer pairs.